Structural Biology and Molecular Biophysics

Conformational dynamics of a nicotinic receptor neurotransmitter binding site

Mrityunjay Singh, Dinesh C. Indurthi, Lovika Mittal, Anthony Auerbach, Shailendra Asthana

Computational Biophysics and CADD Group, Computational and Mathematical Biology Center, Translational Health Science and Technology Institute, NCR Biotech Science Cluster, Faridabad 121001, India • Department of Physiology and Biophysics, University at Buffalo, State University of New York, Buffalo, United States

Reviewed Preprint

Published from the original preprint after peer review and assessment by eLife.

About eLife's process

Reviewed preprint version 1
January 11, 2024 (this version)

Sent for peer review
September 20, 2023

Posted to preprint server
September 17, 2023

Abstract

Agonists activate receptors by interacting more strongly with active versus resting conformations of their target sites. For each ligand, the strong-weak binding free energy difference sets efficacy and the weak/strong ratio sets efficiency. We performed molecular dynamics simulations to explore the conformational dynamics of a nicotinic receptor neurotransmitter binding site in the weak→strong structural transition. The alternative conformations were identified by comparing calculated and experimental binding free energies for 4 agonists. In weak→strong, the agonist rotates about its cationic center (a 'flip'), loop C moves in (a 'flop') to reposition αY190 to form a water-mediated cross-subunit hydrogen bond with the ligand. The flop restructures the aromatic core, and the flip increases van der Waals interactions to generate a more compact, hydrophobic and stable pocket. The simulations reveal a transient intermediate state as well as changes in a salt bridge that may distinguish agonists.

eLife assessment

This **useful** work provides insight into agonist binding to nicotinic acetylcholine receptors, which is the stimulus for channel activation that regulates muscle contraction at the neuromuscular junction. The authors use in silico methods to explore the transient conformational change from a low to high affinity agonist-bound conformation as occurs during channel opening, but for which structural information is lacking owing to its transient nature. The evidence supporting the main conclusion that ligands flip ~180 degrees in the binding site as it transitions from a low to high affinity bound conformation is **incomplete** because little support is available for the starting low affinity docked conformations, and the rather approximate methods for computing binding free energies differ significantly from experimental measures for two of the four tested ligands. Nonetheless, this work presents an intriguing possibility for the nature of a transient conformational change at the agonist binding site correlated with channel opening. If the ligand flip observed in these simulations can be reproduced or verified by other studies, then this work would stand as a significant advance in our knowledge of nicotinic receptor gating.

Introduction

Skeletal muscle nicotinic acetylcholine receptors (AChRs) mediate synaptic transmission between motor neurons and muscle fibers. These pentameric ligand-gated ion channels (pLGICs) are composed of four different subunits (2 α1, β1, δ, and ε) arranged symmetrically around a central ion-conducting pore (Rahman et al., 2020; Unwin, 1993). Binding of the neurotransmitter acetylcholine (ACh) or other agonists to two target sites in the extracellular domain (ECD) increases the probability of a global conformational change that opens a distant (~60Å) channel 'gate' in the transmembrane domain (TMD), to allow water and cations to cross the membrane.

At the start of the channel-opening isomerization the agonist binding sites switch from low to high affinity (LA→HA), and at the end of the isomerization the gate switches from closed to open ($C_{LA} \rightarrow O_{HA}$) (Purohit et al., 2013). Without a bound agonist, the probability of the O shape (P_O) is small and baseline activity is negligible (Jackson, 1986; Nayak et al., 2012; Purohit & Auerbach, 2009). Agonists (A) increase P_O because they provide more favorable binding energy to the target in its active vs resting conformation, making O_{HA} more stable than C_{LA}. Agonists also bind strongly to the transition state that separates O from C and so also increase the channel-opening rate constant (Grosman et al., 2000).

The binding free energy difference between high and low affinity (ΔG_{HA}-ΔG_{LA}) drives receptor activation and determines agonist efficacy, the high-concentration limit of the dose-response curve. In contrast, the binding free energy ratio ($\Delta G_{LA}/\Delta G_{LA}$) generates a correlation between the curve's maximum and midpoint and determine agonist efficiency, the fraction binding energy converted into movements that trigger receptor conformational change.

Adult-type muscle AChRs have an unfavorable unliganded isomerization free energy (+8.3 kcal/mol at −100 mV) (Nayak et al., 2012) and 2 approximately equal and independent binding sites a (Nayak & Auerbach, 2017). For ACh, ΔG_{HA}=-10.2 kcal/mol and ΔG_{HA} =-5.1 kcal/mol per site, so adding their differences at 2 sites to that of the intrinsic isomerization, gives −1.9 kcal/mol. A free energy difference is proportional to the logarithm of an equilibrium constant. Hence, after binding 2 neurotransmitters the AChR gating equilibrium constant increases from 7.4×10^{-7} to 25, and P_O increases from $\sim10^{-6}$ to 0.96 (**Fig. 1A**). Binding energy from 2 neurotransmitters turns the receptor approximately from off to on.

Our goal is to associate $\Delta G_{LA \rightarrow} \Delta G_{HA}$ changes with underlying structural rearrangements at the binding site. Here, we use MD simulations to explore the conformational dynamics of the LA→HA transition at the α-δ neurotransmitter binding site of the *Torpedo* AChR (6UVW; (Rahman et al., 2020)). Binding free energies calculated *in silico* aligned with those estimated experimentally by using electrophysiology, so it was possible to interpret the agonist energy changes with restructuring of the binding pocket. It is difficult to draw sweeping conclusions because we examined only 4 agonists and only one wild-type site. However, in the LA→HA transition for all constructs the agonist somersaults, loop C droops to reposition αY190 and rearrange an aromatic pocket that contracts and becomes more hydrophobic. Also, in all systems the initial LA and final HA conformations of the binding site were connected by a brief intermediate state. For some but not all agonists, loop F moves in and a conserved salt bridge shortens. The results suggest that that agonist mobility is important determinant of the increase in binding free energy, and that rather than acting as a lid that closes, loop C is a positioning device that inserts an affinity-increasing side chain into the pocket core.

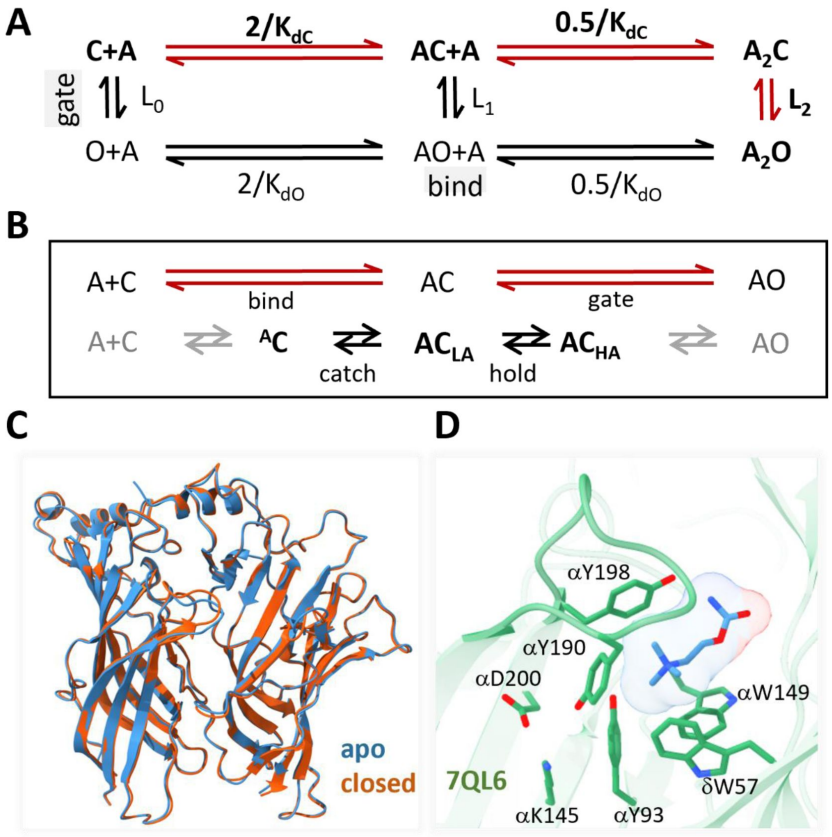

Fig. 1

AChR activation (function and structure)

A. cyclic activation scheme. Vertical, gating. Receptors isomerize between resting (C) and active (O) conformations (equilibrium constant L_n, where n is the number of bound ligands). Horizontal, binding. Agonists (A) bind weakly to C (equilibrium dissociation constant K_{dC}, free energy change ΔG_{LA}) and strongly to O (K_{dO}, ΔG_{LA}). In adult AChRs the 2 sites are equivalent and independent and there is no significant external energy $L_2/L_0 = (K_{dC}/K_{dO})^2$ (Nayak & Auerbach, 2017). B. intermediate steps in binding and gating. Left, the agonist diffuses to the target to form an encounter complex that then becomes a LA complex by a 'catch' rearrangement. Right, The LA site becomes HA by a 'hold' local rearrangement, followed by domain restructurings that eventually generate a conducting pore. Bold, the. free energy changes in catch and hold (ΔG_{LA} and ΔG_{HA}) determine agonist action. *C.* overlay of α and δ subunits extracellular domains, toxin-less (red, 6UWX.pdb) and apo (blue, 7QKO.pdb). There are no major deviations (C_α RMSD = 0.3 Å). D. α-δ subunit neurotransmitter site with CCh (blue) in a HA, desensitized conformation (7QL6.pdb; (Zarkadas et al., 2022)). The agonist is in the *trans* orientation (tail points towards δ).

Results

Hold

Traditionally, receptor activation is divided into binding (formation of a ligand-protein complex) and gating (receptor isomerization). Here, we are concerned only with movements at binding sites that connect these two steps. In binding, the agonist (A) diffuses to interact with the target ($A+C=^{A}C$), after which a local rearrangement establishes the LA complex ($^{A}C=AC_{LA}$) (Jadey & Auerbach, 2012). In gating, the site again rearranges to produce the HA complex ($AC_{LA}=AC_{HA}$), after which the rest of the protein domains (ECD, TMD and gate) restructure to establish AO_{HA}. We call the two local rearrangements of the binding site 'catch' (free energy change ΔG_{LA}) and 'hold' (ΔG_{HA}-ΔG_{LA}) (**Fig. 1B**). The end of binding is AC_{LA} and the start go gating is AC_{HA}, so hold is the local rearrangement that connects these two activation steps.

The free energy changes associated with the other events in binding and gating, namely diffusion to the site (the chemical potential) and restructuring of receptor domains, are the same for the agonists we have examined and so are not relevant to this study. Furthermore, energy coupling between the binding pocket and distant residues (>15 Å) typically is weak (Gupta et al., 2017) (Fig. S1A). Only catch and hold determine differences between agonists with regard to affinity (ΔG_{LA}, ΔG_{HA}), efficacy (ΔG_{HA}-ΔG_{LA}) and efficiency ($1-\Delta G_{LA}/\Delta G_{HA}$) (Nayak et al., 2019). In AChRs, ΔG_{LA} and ΔG_{HA} have been measured experimentally for 23 agonists and 53 binding site mutations (Indurthi & Auerbach, 2023) (Fig. S1B). The structures generated in the MD simulations were identified as AC_{LA} or AC_{HA} by aligning ΔG_{LA} and ΔG_{HA} values calculated i*n silico* with those from experiments.

The cryo-EM structures of AChRs include apo, resting-C with a bound toxin and high-affinity desensitized (Rahman et al., 2022; Rahman et al., 2020; Zarkadas et al., 2022). Binding sites of desensitized AChRs have a similar (perhaps identical) high affinity as do O sites (Auerbach, 2020). The end states of the hold rearrangement are short-lived and have not been captured as structures.

Because ΔG_{LA} and ΔG_{HA} are independent of energy changes outside the binding pocket, in the simulations we removed the TMD and studied only α-Δ subunit ECD dimers. The starting structure for the hold transition was (PDB: 6UWZ) after toxin removal that is essentially the same as the apo structure (Zarkadas et al., 2022)) (**Fig. 1C**). The 4 agonists we examined were acetylcholine (ACh), carbamylcholine (CCh), epibatidine (Ebt) and epiboxidine (Ebx).

Docking

Binding energy changes in hold, $AC_{LA}=AC_{HA}$ (**Fig 1B**). To understand the structural underpinnings, we began by removing α-bungarotoxin from the high-resolution (2.69 Å) structure 6UWZ (Rahman et al., 2020) and docking agonists into the empty pocket at the α-δ subunit interface (**Fig. 1C**). The docking simulations had strong binding scores, ranging from −5.82 to −9.18 kcal/mol, suggesting stable interactions. However, unlike the agonist orientation apparent in cryo-EM structures of desensitized AChRs (Gharpure et al., 2019; Noviello et al., 2021; Rahman et al., 2022; Walsh et al., 2018; Zarkadas et al., 2022) (**Fig. 1D**), the agonist's tail pointed away from (*cis*) rather than towards (*trans*) the complimentary (non-α) subunit. This was the case for the top 3 docking scores for all 4 ligands (**Fig. 2A**). Because the *cis* orientation was not observed in any cryo-EM (HA) structure, we examined the top 200 docking scores for CCh. All poses were *cis*, with the tail pointing towards the α subunit. The *cis* orientation was also apparent in docking of agonist into a putatively LA binding site of a homology model (Tripathy et al., 2019). To start, we associated the agonist orientation in the hold end states as *cis* in AC_{LA} versus *trans* in AC_{HA}.

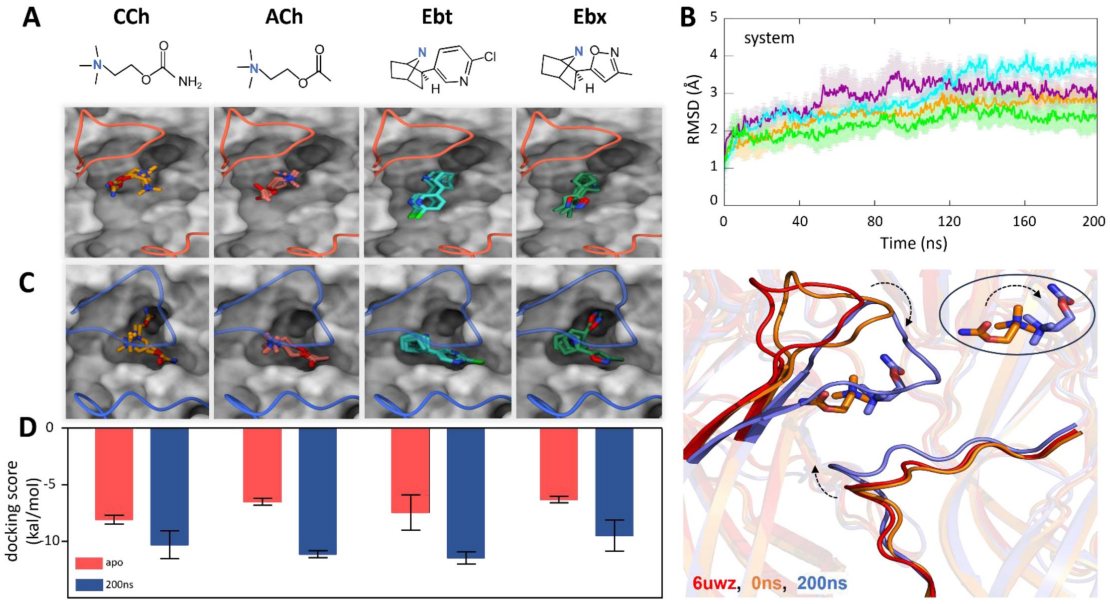

Figure 2.

Agonist docking and dynamics

A. *top,* Agonist structures (blue, main N^+): carbamylcholine (CCh), acetylcholine (ACh), epibatidine (Ebt) and epiboxidine (Ebx). B. *top*, root-mean-square-deviation (RMSD) of the system C_α (mean±SD, triplicates) throughout 200 ns MD simulations (ACh, cyan; CCh, green; Ebt, orange; Ebx, purple). *bottom*, close-up view of the pocket showing movements during MD simulations with CCh (red, apo; orange, 0 ns; blue, 200 ns;). Loop C moves down, loop F closes in, the agonist rotates *cis*→*trans.* C. α-Δ binding pocket (6UVW.pdb minus toxin) with agonists (top 3 poses). *top*, docked into the 0 ns structure (red). Loop C is up, loop F is out, agonist is *cis*. *bottom*, docked into the 200 ns structure after removing CCh (blue). Loop C is down, loop F is in and the agonist is *trans*. D. Docking score energies (mean±SD), 0 ns (red) and 200 ns (blue) suggest a LA→HA transition during the course of the simulation.

LA → HA transition

We performed 200 ns MD simulations for each of the docked complexes, in triplicate (with different seed values) (**Fig. 2B** top). The MD simulations for all three replicates demonstrated similar root-mean-square-deviation (RMSD) patterns, with differences consistently below 1Å (Table S1) suggesting that the trajectories were robust and reproducible. Although there were initial deviations, all systems became stable by ~120 ns. The root-mean-square-fluctuation (RMSF) of the C_α atoms, employed to identify regions of flexibility, showed instability mainly in loops C and F around the pocket (Fig. S2). The fluctuations observed at the base of the ECD were anticipated because the TMD that offers stability here was absent.

In addition to the fluctuations in these loops, during the 200 ns simulations the ligand orientation changed dramatically, *cis*-to-*trans*. At the start of the simulations the agonist's tail points towards α, and at the end it points towards δ (**Fig. 2B** bottom). This rearrangement represents a substantial rotation (a 'flip') about the agonist's main cationic center (N^+) that remains close to αW149 throughout the somersault. The final MD configuration (with CCh) was well-aligned with the CCh-bound cryo-EM desensitized structure (7QL6.PDB) (RMSD < 0.5 Å) (Fig. S3), further demonstrating that the simulation had converged.

To test whether rearrangements at the binding pocket in the simulations themselves enforce the *trans* configuration, we removed the bound CCh from the final state MD structure and re-docked all four agonists. The preferred poses for all 4 agonists were all *trans* (**Fig. 2C**). In addition, binding energies from docking scores were higher for the converged MD structure compared to the initial binding site structure. As a further control we carried out MD simulations of a pentamer docked with ACh and found similar structural changes at the binding pocket compared to the dimer (Fig. S4). These results indicate that a dimer is appropriate to study local rearrangements of an AChR neurotransmitter binding site and suggest that in the MD simulations the binding site restructures from AC_{LA} to AC_{HA} conformation (**Fig. 2D**).

Principal component analysis

To identify the most prominent conformational states of the receptor during the MD simulations, principal component analysis (PCA) was carried out based on the most significant fluctuations (principal components). Considering the first two principal components (PC-1 and PC-2) that capture the most pronounced C_α displacements, the protein backbone fluctuations revealed three energy minima (m1, m2, and m3) that mainly reflect the stabilities of loops C and F (**Fig. 3**). For all four agonists, the trajectories quickly reach m1 (≤20 ns), then transition through m2, and culminate in m3 (180-200 ns). In the simulations progress in time was sequential, m1 → m2 → m3.

Accordingly, we hypothesized that m1 corresponds to AC_{LA} and m3 corresponds to AC_{HA}. For all agonists, the m2 population has greater variance (more instability) compared to m1 and m3. This, along with its position in the sequence, suggests that m2 represents an unstable intermediate configuration within hold, between AC_{LA} and AC_{HA}. For all agonists and trajectories, m3 had the least variance (was most stable), again supporting convergence by 200 ns.

Transitions between the 3 energy minima varied with the agonist. Always, m1 was apparent first (at 5-14 ns for ACh; 15-24 ns for CCh; 21-41 ns for Ebt; 20-56 ns for Ebx), followed by m2 (20-50 ns; 50-60 ns; 60-100 ns; 100-120 ns). All systems converged to m3 (180-200 ns) (**Fig. 3**). The bottom of the m1, m2 and m3 energy wells represent the most stable configurations of each population and serve as a reference point for the rest of energy well.

Although the bottom of the well for 3 energy minima from PCA represent the most stable overall conformation of the protein, they do not convey direct information regarding agonist stability or orientation. To incorporate this information, we performed a cluster analysis of the ligand using frames from the bottom of each PCA well as inputs. The top three clusters, each having RMSD of ≤

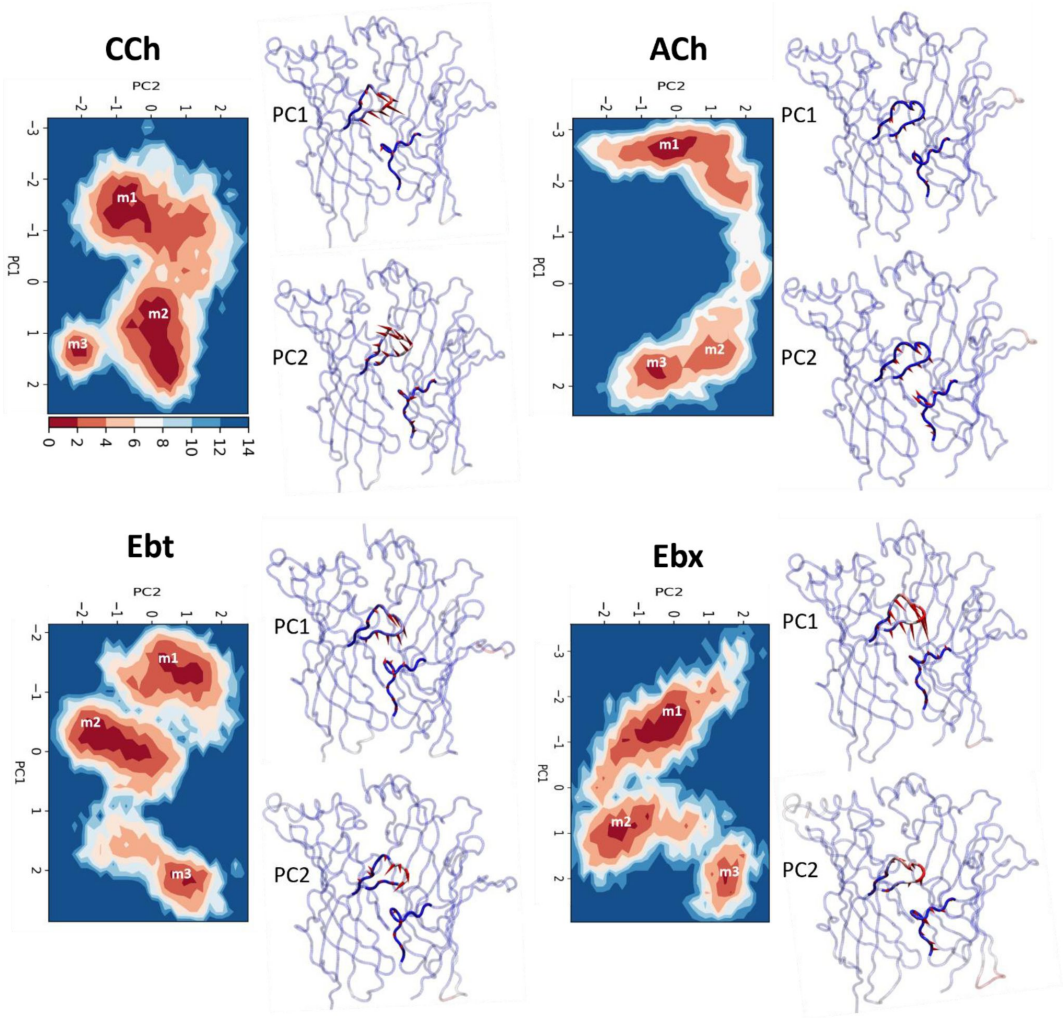

Figure 3.

Principal Component Analysis (PCA)

For each agonist, the left panel plots PC1 vs PC2, the first two principal components that capture the maximum variance in the trajectory. Colors represent free energy value in kcal/mol (upper left, bottom). For all agonists there are 3 energy minima (red), m1, m2, and m3, that correspond to different conformations of the protein-ligand complex. The right panels are 'porcupine' plots that indicate the direction and magnitude of changes between PC1 and PC2. In order of appearance, m1 (≤20 ns)< m2<m3 (≥180 ns) (see text). m1 represents AC_{LA}, m3 represents AC_{HA}, and m2 is an intermediate configuration (corresponding ΔGs given in **Table 1**).

		window (ns)	n clusters	ΔH (SD, SEM)	TΔS (SD, SEM)	ΔG calculated	ΔG experimental	η calculated	η experimental
	m1	15-24	226	-27.61 (7.66, 0.49)	-22.88 (5.82, 2.37)	-4.73	-4.44		
CCh	**m2**	100-120	273	-24.41 (5.68, 0.79)	-17.54 (3.49, 1.42)	-6.87		0.52	0.52
	m3	186-200	207	-26.18 (5.75, 0.47)	-16.25 (7.76, 2.24)	-9.93	-9.20		
	m1	5-14	100	-20.83 (8.11, 1.13)	-14.27 (6.51, 3.25)	-6.56	-5.11		
ACh	**m2**	20-50	359	-27.92 (3.01, 0.29)	-16.72 (2.53, 1.03)	-11.2		0.47	0.50
	m3	160-200	266	-27.00 (2.88, 0.87)	-14.57 (6.28, 3.63)	-12.43	-10.31		
	m1	21-41	591	-27.64 (3.83, 0.27)	-13.42 (4.70, 1.42)	-14.22	-6.20		
Ebt	**m2**	50-60	325	-24.21 (4.25, 0.42)	-13.50 (6.81, 2.05)	-10.71		0.42	0.42
	m3	175-200	996	-41.77 (3.99, 0.28)	-17.23 (6.86, 2.07)	-24.54	-10.60		
	m1	20-56	1284	-20.51 (2.98, 0.46)	-12.85 (5.49, 1.66)	-7.66	-5.40		
Ebx	**m2**	60-100	504	-21.55 (3.56, 0.28)	-14.39 (10.46, 3.15)	-7.16		0.48	0.46
	m3	174-200	562	-33.95 (2.92, 0.88)	-19.33 (4.39, 1.32)	-14.62	-9.96		

Agonists, see Fig. 2A. For the *values* calculated *in silico*, frames from each PCA population (m1, m2 and m3; Fig. 3) were selected after cluster analysis of ligand orientation. Methods for the experimental energy values are described elsewhere (Indurthi & Auerbach, 2021). window, frame times for each population; ΔH, change in binding enthalpy; ΔS change in binding entropy (T, absolute temperature); ΔH, change in Gibbs free energy (ΔG=ΔH -TΔS); η, efficiency ($1-\Delta G_{LA}/\Delta G_{HA}$). SD, standard deviation; SEM, standard error of mean.

Table 1.

Calculated and experimental binding energies (kcal/mol)

1Å, shared a similar ligand orientation (Fig. S5) and were selected to compute binding free energy using MM-PBSA. The remaining frames were disregarded. The fraction of frames accepted for free energy calculations ranged from a minimum of 20% (ACh, m1) to a maximum of 71% (Ebt, m3). On average, the fraction of frames selected from each energy minimum was ~50%, showing the dynamic nature of the ligand in the pocket (**Table 1**).

Computed vs experimental binding energies

The above procedure defined populations of structures that we hypothesize represent the end states of hold, AC_{LA} (m1) and AC_{HA} (m3), plus an intermediate (m2). We used MM-PBSA (Molecular Mechanics Poisson-Boltzmann Surface Area) computations of the selected structures to estimate binding energy of each agonist to each population. MM-PBSA is particularly useful to compare binding affinities between different states and among agonists (Kollman et al., 2000; Rastelli et al., 2010; Sun et al., 2014). In our use, MM-PBSA computations included both enthalpic (ΔH) contributions from molecular interactions (van der Waals, electrostatics, solvation) and entropic (TΔS) contributions calculated using normal mode analysis. By capturing the dynamic interplay between the ligand and receptor as well as the influence of the surrounding solvent environment this approach enables computation of a Gibbs free energy (ΔG). However, there are limitations with regard to MM-PBSA accurately predicting absolute binding free energies (Genheden & Ryde, 2015; Hou et al., 2011) that depends on parameterization of the ligand (Oostenbrink et al., 2004).

The calculated and experimental ΔG values are shown in **Table 1**. For ACh and CCh, there is good agreement between ΔG_{m1} and ΔG_{LA} and between ΔG_{m3} and ΔG_{HA}. For these agonists, *in silico* values overestimated experimental ones only by ~8% and ~25%. The agreement was not as good for the other 2 agonists, as calculated values overestimated experimental ones by ~45% (Ebt) and ~130% (Ebt). However, the fractional overestimation was approximately the same for ΔG_{LA} and ΔG_{HA}.

Despite these discrepancies in absolute values, the trend of an increase in binding free energy, m1 versus m3, is consistent with the assignment, AC_{LA} versus AC_{HA}. For all agonists, the stability of the ligand-receptor complex increases significantly in the m1→m3 transition (**Fig. 4A**). Further support for the assignment is from comparing calculated vs experimental efficiencies (η) that depend on $\Delta G_{LA}/\Delta G_{HA}$ (Nayak et al., 2019). Table 2 shows that η values calculated *in silico* agree closely (≤5%) with those measured experimentally, for all agonists. Apparently, MD simulations of a single pdb file successfully model the hold transition. The match between calculated and experimental efficiencies is evidence that that m1 represents low-affinity AC_{LA} and m3 represents high-affinity AC_{HA}.

In the $AC_{LA} \rightarrow AC_{HA}$ conformational change, all agonists show an increase in van der Waals (vdW) interaction energy. The increase was most pronounced with Ebt (−9.77 kcal/mol) and least for Ebx (−3.54 kcal/mol), with CCh (−8.81 kcal/mol) and ACh (−6.71 kcal/mol) falling in between (**Fig. 4**, Table S2). Also, in $AC_{LA} \rightarrow AC_{HA}$, restructuring of the binding pocket further contribute to generating a smaller, more-tightly packed pocket. This is shown in **Fig. 4C** as a reduction in binding pocket volume and in **Fig. 4D** as a decrease in the number of water molecules. The agonist's flip into the pocket results in de-wetting and a more hydrophobic environment.

Flip-Flop

The ligand somersault (flip) was prominent in all simulations of hold. All agonists undergo a large rotation about the N^+-αW149 fulcrum (**Fig. 5**; Video 1). The extent of rotation was 131° for CCh, 156° for ACh, 148° for Ebt and 176° for Ebx. Another consistent and prominent restructuring event in $AC_{LA} \rightarrow AC_{HA}$ was the downward displacement (flop) of loop C toward the core of the pocket. This movement is conserved in related receptors and thought to play a role in receptor activation by agonists (Basak et al., 2020; Hansen et al., 2005; Hibbs et al., 2009) (see below). In the

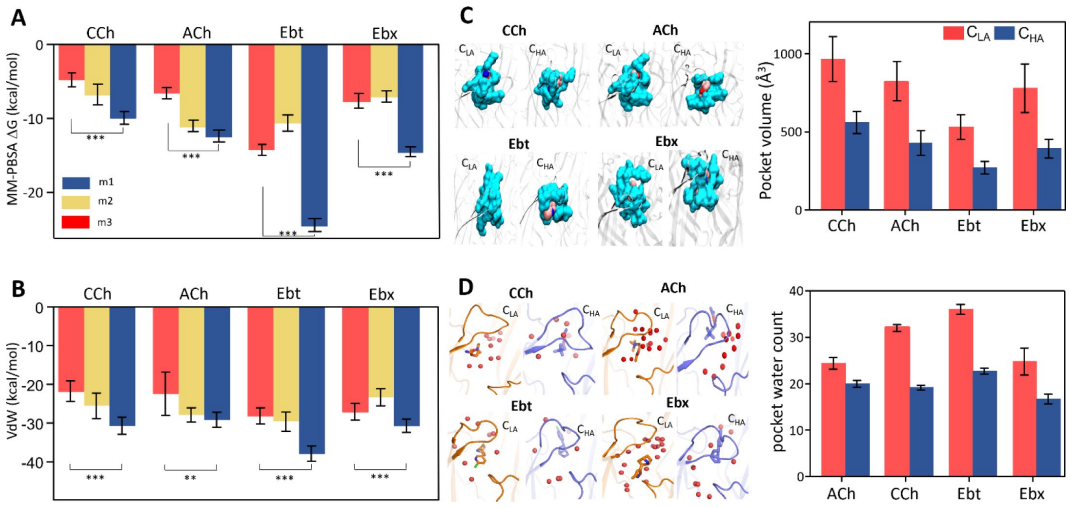

Figure 4.

Binding free energies and pocket properties

A. Calculated Gibbs free energy (ΔG) using MM-PBSA for the three distinct energy minima (m1, m2, and m3) showing the progression LA to HA (agonists, **Fig. 2A**). ΔG_{m2} is intermediate for ACh and CCh but least stable for Ebt and Ebx. B. vdW interactions increase m1 (AC_{LA}) to m3 (AC_{HA}), consistent with increased hydrophobicity. C. Binding pocket volume reduces m1 to m3, reflecting the more tightly packed pocket in AC_{HA}. D. The number of water molecules in the pocket decreases m1→m3, orange, C_{LA}; blue, C_{HA}, reflecting a more hydrophobic environment in AC_{HA}.

simulations, we quantified loop C flop by measuring the displacement of its tip (C_α of αC192) relative to its starting position (at 0 ns). The distance traveled at 200 ns varied with the agonist and was 9.2 Å for CCh, 5.5 Å for Ebt, 5.2 Å for ACh and 3.3 Å for Ebx (**Fig. 5**). We do not discern a pattern with regard to agonist affinity, efficacy or efficiency.

In hold, residues that form the pocket cavity move, apparently to accommodate the re-orientation of the ligand. In AC_{LA} αY190, αY93, and δW57 are spaced apart, providing an open slot that accommodates the agonist's tail in the *cis* orientation. However, in AC_{HA} αY190 is positioned closer to αY93, effectively creating a unified surface that disallows the *cis* position of the tail (Fig. S6). However, in the simulations the event sequence is not clear so perhaps flip precedes flop, and agonist re-orientation first creates the space for αY190 to occupy.

αW149 (in loop B) makes a cation-π bond with N^+ that is important for ligand stabilization (Xiu et al., 2009; Zhong et al., 1998). In the simulations, the position and orientation of αW149 relative to N^+ remained almost unchanged for all 4 agonists, in both AC_{LA} (*cis*) and AC_{HA} (*trans*) configurations (**Fig. 6**). Apparently, the cation-π bond acts as a slippery anchor that maintains stability of the N^+ position even as the tail rotates about it.

Loop C flop results in re-positioning of αY190 into the aromatic pocket. αY190 is the main ligand binding energy source, nearly twice as strong as αW149 (Purohit et al., 2014), perhaps because deprotonation of its hydroxyl group generates a cation-anion bond with N^+ (Bruhova & Auerbach, 2017). An interaction between αY190 and the αK145-αD200 salt bridge, suggested to be the trigger for the gating isomerization (Bruhova & Auerbach, 2017; Mukhtasimova et al., 2005). In $AC_{LA} \rightarrow AC_{HA}$, loop C flop restructures the pocket to put N^+ between the αY190 and αW149 rings, and αY190 closer to the salt bridge (**Fig. 6**).

Other hold rearrangements

In AC_{LA} (m1), the *cis* orientation is stabilized by the hydroxyl of αY93 that is proximal to a functional group on the agonist tail. Also, the tail nitrogen in CCh, Ebt, and Ebx (amide or amine) forms a hydrogen bond with the hydroxyl group of αY198, but only in the intermediate m2 state. This interaction appears to guide the flip and provide transient stability to the intermediate state. The absence of a secondary nitrogen in ACh possibly explains its alternate re-orientation route, as only this ligand was observed to flip counterclockwise (**Fig. 5**). It may also explain why the m2 basin in the PCA plots for ACh is especially broad and shallow (**Fig. 3**).

In AC_{HA} (m3), the αY190/αY198/δW57 rings and the αW149 indole interact with N^+, and the hydroxyl group of αY93 forms a hydrogen bond with the ligand head group (Celie et al., 2004; Hansen et al., 2005). However, Ala substitutions of these 5 aromatic residues have quite different consequences and result ACh binding free energy losses of +4.4, +1.9, +0.1, +2.3 and +0.9 kcal/mol, respectively (Purohit et al., 2014). In AC_{HA}, the tail functional moiety (carbonyl or secondary ring amine) in the *trans* orientation is sandwiched between αC192, αC193 and αY198 (loop C), αT150 (loop B) and δC108, δN109, δL111, and δL121 (loop E) (Fig. S7).

αK145 is complex and undergoes agonist-dependent hold rearrangements. In AC_{HA} this residue i) makes a salt bridge with αD200, ii) has a cation-π interaction with αY93, iii) contacts αY190 (possibly through the hydroxyl group) and iv) approaches loop F of the complementary subunit (Zarkadas et al., 2022). Further, the mutation αK145A lowers the efficiencies of ACh and CCh (from 0.51 to 0.41) but has no effect on those of Ebt and Ebx (0.41) (Indurthi & Auerbach, 2023).

This agonist dependence with regard to function has a parallel in structure. In the hold simulations, the αK145-αD200 distance (Å) increases from 4.4 in apo to 6.1 or 5.1 in AC_{LA} (CCh or ACh). The spread may relate to the agonist tail being inserted into the αY93 slot in the *cis* orientation. In $AC_{LA} \rightarrow AC_{HA}$, for some agonist the αK145-αD200 distance (Å) shortens substantially to 2.6 or 2.8, making the bridge more rigid (ACh or CCh). However, with Ebt and Ebx the αK145-

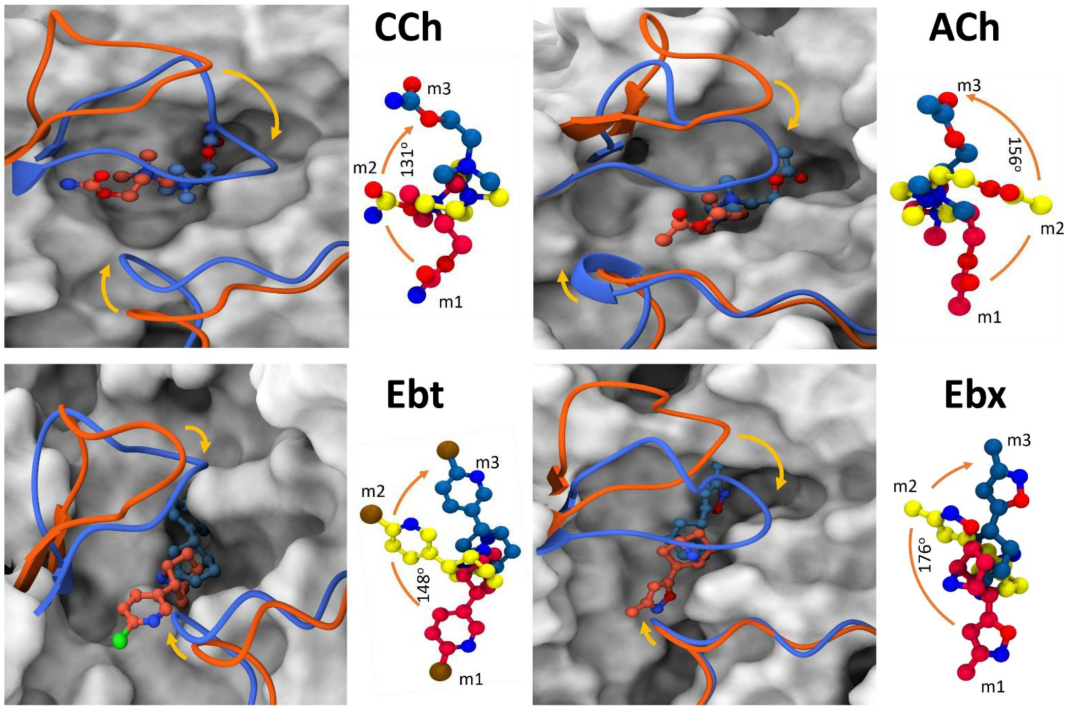

Figure 5.

Agonist and loop movements in hold

In each panel, *left*, superimposed cartoons of AC_{LA} (m1; orange) and AC_{HA} (m3; blue). Loop C is upper left and loop F is lower right. In $AC_{LA} \rightarrow AC_{HA}$ (orange → blue) there is a *cis* → *trans* reorientation of the agonist (a flip) and a downward movement of loop C (a flop). *right*, the degree of flip from m1 (red) to m2 (yellow) to m3 (blue). The range, m1 (AC_{LA}) → m3 (AC_{HA}), is 131° to 176°.

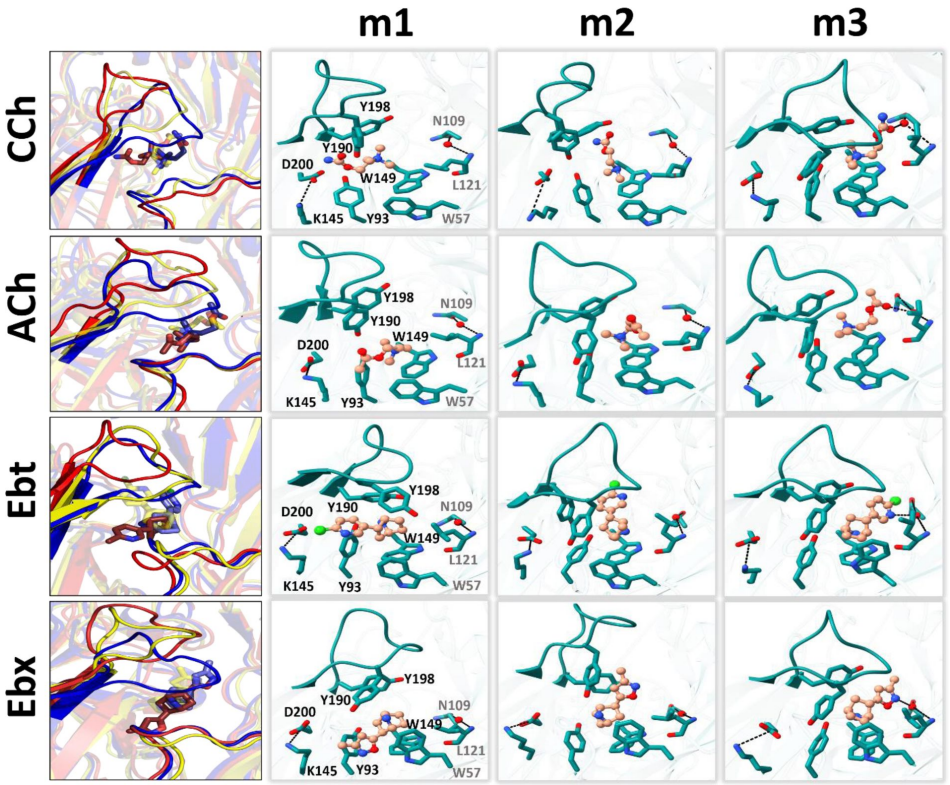

Fig. 6

Representative snapshots in hold

left, rearrangements of loop C, loop F and the ligand (m1, red; m2, yellow; m3, blue). Right, conserved residues and ligand orientation. m1 is AC_{LA} and m3 is AC_{HA}. In m1, a functional group at the agonist tail interact with αY93 (all agonists) and αD200 (CCh and Ebt). The position and orientation of αW149 relative to N^+ of the agonist remains unchanged m1 → m3 and serves as a fulcrum for the *cis* → *trans* flip (see **Fig. 5**). In m2, the functional nitrogen at the agonist tail (CCh, Ebt and Ebx) interacts with the hydroxyl group of αY198. For all ligands, loop C flop (m1 → m3) repositions αY190 in pocket. In m3, the agonist fully flips to *trans*, facilitating the interaction of N^+ with αY190 and the formation of water-mediated hydrogen bond with the reactive group at the tail with δN109/δL121 (loop E).

αD200 distance remains unstable, fluctuating between 3-6 Å throughout the course of the simulation. Likewise, αK145-αY190 distance stabilizes at 5.3 Å or 6.1 Å in AC_{HA} with ACh and CCh but continues to fluctuate with Ebt and Ebx. In contrast, the αY190-αD200 distance remains stable in AC_{HA} for all ligands. This suggests that the instability in the salt αK145-αD200 and αK145-αY190 distances can primarily be attributed to αK145 (Fig. S8).

In AC_{HA}, the functional group found in the tail of each agonist -- the carbonyl group in CCh and ACh and the secondary ring amine in Ebt and Ebx - forms a hydrogen bond with the carbonyl of δN109 and the amine of δL121 in the complementary δ subunit *via* a structural water (**Fig. 6**), as reported elsewhere (Blum et al., 2010; Gharpure et al., 2019; Zarkadas et al., 2022). This water-mediated bonding appears to be crucial for stabilizing the agonist in the *trans* orientation. The start of the agonist's flip, m1→m2, begins the establishment of this water-mediated bond that is completed in m2→m3, with all 4 agonists (**Fig. 6**).

Discussion

In diffusion-catch-hold activation of AChRs ($A+C \rightleftarrows {}^{A}C \rightleftarrows AC_{LA} \rightleftarrows AC_{HA}$; **Fig. 1B**), the binding free energy increase in the last step generates the force that initiates the receptor isomerization. We identified in MD simulations (**Fig. 3**) the hold end states, AC_{LA} (m1) and AC_{HA}, (m3), as well as an intermediate configuration (m2). Our approach to understanding the conformational dynamics of hold is to compare calculated with experimental binding free energies, ΔG_{LA} and ΔG_{HA}. There are many experimental measurements for many different AChR agonists and several binding sites (Indurthi & Auerbach, 2023; Jadey & Auerbach, 2012; Purohit et al., 2014), but here we describe the comparison for only 4 agonists and only the wt α-δ site.

The alignment between experimental and calculated free energies was closer for ACh and CCh than for Ebt and Ebx (**Table 1**). The match improved when free energy ratios rather than absolute values were compared. Individual *in silico* values overestimated experimental ones by approximately the same factor (different for each ligand) that, however, cancelled in the ratio. We do not know the origin of this factor but speculate that it could be caused by errors in ligand parameterization. Regardless, the results show that agonist efficiency (η) can be estimated from only agonist and receptor structure (one PDB file), and that η is a useful metric for associating structure with function.

In the $AC_{LA} \rightarrow AC_{HA}$ simulations, two conspicuous binding site rearrangements were a *cis*→*trans* somersault of the agonist (a flip) and an up→down droop of loop C (a flop). The loop C movement is well known, but its functional role has been puzzling. The extent of the flop is correlated with agonist potency in ACh binding proteins (Basak et al., 2020; Du et al., 2015; Polovinkin et al., 2018), but voltage-clamp fluorometry of other receptors shows it to be similar with agonists and antagonists (Chang & Weiss, 2002; Munro et al., 2019; Pless & Lynch, 2009). In AChRs, truncation of loop C prevents activation by agonists but has no effect on unliganded activation, but agonist sensitivity is maintained if αY190 and αY198 are intact (Purohit & Auerbach, 2013). These results suggest that the downward displacement of loop C in AChRs is mainly associated with the generation of strong binding energy.

Perhaps the most puzzling result regarding loop C is that the agonist association rate constant k_{on} is slower to AC_{LA} (up position) than to AC_{HA} (down position) (Grosman & Auerbach, 2001; Nayak & Auerbach, 2017). Moreover, whereas k_{on} to AC_{LA} is correlated with agonist potency (the dissociation rate constant k_{off} is approximately the same for all agonists), k_{on} and k_{off} to AC_{HA} both are agonist dependent. The flop of loop C in hold removes a barrier to make k_{on} approximately diffusion-limited, and also reduces discrimination between ligands (molecular recognition.

Loop C droop resembles the 'clamshell closure' apparent at other receptors binding site (Chen et al., 2017; Hansen et al., 2005; Hibbs & Gouaux, 2011). However, in the light of the above experimental results, this label is misleading because 'closing' (or 'capping') a binding pocket is expected to slow rather than speed k_{on}. For this reason, we use less functionally loaded words to describe the downward displacement of loop C, namely a 'flop' or 'droop'. In $AC_{LA} \rightarrow AC_{HA}$ loop C indeed moves closer to αC of αW149, to cover the pocket and create higher affinity. However, it does not do so by imposing a steric barrier. We did not study the catch rearrangement and do not speculate about the nature of the barrier that limits the agonist association rate constant to C_{LA} that has loop C in an up position.

Importantly, loop C flop repositions αY190, the main determinant of both LA and HA binding energies (Bruhova & Auerbach, 2017; Purohit et al., 2014). In $AC_{LA} \rightarrow AC_{HA}$, this side chain fills the slot adjacent to αY93 that otherwise allows the *cis* orientation in AC_{LA} (Fig. S5). Further, flop moves αY190 closer to a salt bridge between αK145-αD200, and compacts the space between αW149 and N^+ (**Fig. 6**). Overall, the simulated structures suggest that loop C flop increases binding energy both by repositioning αY190 near N^+ and by allowing the *cis-trans* flip of the ligand. Rather than closing a door, the downward movement of loop C rearranges the furniture.

We interpret *cis-trans* rotation of the agonist about the N^+-αW149 fulcrum (**Fig. 5**) with caution. Although the *trans* orientation is apparent in desensitized AChR cryo-EM structures, the *cis* orientation exists only *in silico*. Notwithstanding this limitation, in $AC_{LA} \rightarrow AC_{HA}$ the agonist's flip into the binding pocket and the repositioning αY190 by loop C flop were observed consistently in all simulations with all agonists, and rationalize the increase binding energy in the hold transition. We speculate that the agonist flip triggers the rest of the hold restructuring but cannot rule out flop promoting flip or synchronous rearrangements. We have been unable to establish clearly the flip-flop temporal sequence.

For the agonists we examined, the somersault positions the tail deep into the binding cavity where it interacts *via* a structural water with the complementary subunit. It appears that agonists rotation increases binding free energy by displacing water and increasing vdW interactions and protein stability. A hydrophobic binding pocket is associated with functional activation in other ion channels (Furukawa et al., 2005; Sigel & Steinmann, 2012) and is observed in many proteins including β2-adrenergic receptor, opioid receptors, and HIV-1 protease (Huang et al., 2015; Rasmussen et al., 2011; Wlodawer & Erickson, 1993). However, these effects on the AChR pocket cannot be the only basis for the higher affinity AC_{HA} because several potent agonists lack a tail, for example tetramethylammonium. We hypothesize that both the reorganization of the aromatic groups in the pocket around N^+ and binding site compaction/de-wetting contribute to stronger binding, in proportions that remain to be determined. Regardless, the agonist's somersault shows that mobility is one feature that distinguishes a ligand from a covalently linked side chain (Indurthi & Auerbach, 2023). Not only can an unconnected agonist come and go, it can also reposition itself dramatically to induce a conformational change of binding pocket to affect a change in binding energy.

Movements analogous to flip and flop have been identified in other proteins. Multiple ligand positions in a binding pocket have been documented in 5-HT3 receptors (Basak et al., 2020), δ-opioid receptors (Shang et al., 2016), HIV-1 protease (Klei et al., 2007) and transthyretin (Klabunde et al., 2000). In enzymes, substrate motion has been observed in hexokinase (Bennett & Steitz, 1978) and alcohol dehydrogenase (Plapp, 2010). Regarding flop, substrate-induced loop displacements are known to reposition residues to enhance catalysis, for example in chymotrypsin (Ma et al., 2005) and triosephosphate isomerase (Brown & Kollman, 1987; Nickbarg et al., 1988). The agonist flip and loop C flop in AChRs are additional examples of ligand mobility and loop motions undergirding function.

The PCA plots (**Fig. 3**) show 3 structural populations, one of which (m2) occurs in time between m1 (AC_{LA}) and m3 (AC_{HA}). In m2, the agonist tail interacts with αY198, possibly to guide the clockwise rotation of the ligand and reduce the probability of a return to the *cis* orientation. ACh was the only agonist to rotate counterclockwise, perhaps because it lacks the appropriate functional group in its tail. The MM-PBSA calculations indicate that ΔG_{m2} (that does not have an experimental correlate) is intermediate between ΔG_{LA} and ΔG_{HA} for ACh and CCh, but least stable for Ebt and Ebx (**Table 1**). We do not have an explanation for this difference. However, we observe m1→m2, m2→m1, m2→m3 and m3→m1 transitions in the trajectories (Video 1), so the depth of the m2 energy well (relative to the barriers that separate it from m1 and m2) contributes to agonist efficacy and efficiency.

MD simulations did not reveal an interaction between the αK145-αD200 salt bridge distance and the degree of loop C displacement (Cheng et al., 2006). However, this distance discriminate between η classes by decreasing $AC_{LA} \rightarrow AC_{HA}$ in high (ACh and CCh) but not in low (Ebt and Ebx) η classes, consistent with experimental results (Indurthi & Auerbach, 2023). All 4 agonists are high efficacy, so this result suggests that perturbation of this salt bridge is not a necessary requirement for the change from LA to HA. After loop C flop, the repositioned αY190 connects N^+ to the salt bridge, suggesting that this interaction (rather than bridge tightening) could help trigger the gating transition (Beene et al., 2002; Gay & Yakel, 2007; Mukhtasimova et al., 2005; Padgett et al., 2007; Pless et al., 2011). The simulation did not reveal the conformational changes (forces) that drive the next step of the isomerization (ECD restructuring). However, the observation that for all agonists, interactions with the complementary subunit and pocket dehydration terminated (at 200 ns) the hold rearrangement lead us to speculate these may contribute.

Loop E (connecting β5 and β6 strands) has been implicated in ligand discrimination (Basak et al., 2020; Muroi et al., 2009; Pless & Lynch, 2009). The double mutation F106L+S108C in the β2 subunit of the α4β2 nicotinic AChR subtype significantly decreases the action of Ebt without altering that of ACh (Tarvin et al., 2017). Loop E residues are responsible for the binding energy difference of α-γ versus α-Δ interfaces because hydrogen bonds influence the position and participation of γW55 (Nayak et al., 2016), and for reducing instability of the α-Δ site consequent to loop C mutations (Purohit & Auerbach, 2013). MD simulations with more agonists and more binding sites are needed to elucidate the role of loop E in the $AC_{LA} \rightarrow AC_{HA}$ transition.

Agonists belong to efficiency (η) classes in which $\Delta G_{LA}/\Delta G_{HA}$ is the same for all members. So far 5 η-classes have been identified experimentally in adult-type AChRs, indicating that are 5 pairs of AC_{LA}/AC_{HA} structures (Indurthi & Auerbach, 2023). Although in the simulations loop F movements and salt bridge distances were agonist dependent, with only 4 ligands we cannot associate these rearrangements with η classes.

The key requirement for allostery is that ligand binding energy be weaker to the resting versus active conformation of the target. Natural selection must generate both low and high affinity binding sites, so our attention must be on restructuring in both $^{A}C=AC_{LA}$ (catch) and $AC_{LA}=AC_{HA}$ (hold). What prevents loop C flop in apo? What barrier(s) slows k_{on} to apo? Where is the agonist in the encounter complex? What forces promote the *cis* orientation? What is the role of water in agonist orientation, both *cis* and *trans*? What are the mechanisms and consequences of a wider salt bridge, apo versus AC_{LA}? What structural classes are associated with efficiency classes? The correlation in the free energy changes in catch and hold that entangles binding with gating implies a corresponding correlation in structural change. We anticipate that additional MD simulations of catch, hold, and post-hold domain rearrangements, for more agonists and with binding site mutations, will lead to a more complete understanding of how agonists turn on the AChR.

Materials and Methods

Hardware and Software

All computational studies were carried out on a Linux Ubuntu 20.04 based workstation with 126 GB RAM, 64 CPU cores, and two RTX A5000 24 GB GPU cards, as well as an Ubuntu 20.04 based server equipped with 132 GB RAM, 96 CPU cores, and two RTX A5000 24 GB GPU cards. The software utilized includes the Maestro release 2022-2 graphical user interface (GUI) of the Schrödinger software suite (BioLuminate, Schrödinger, LLC, NY, USA), Amber22 (Case et al., 2005), VMD 1.9.3 (Humphrey et al., 1996), ChemDraw Professional 15.1 (Purushotham et al., 2022), ChimeraX (Pettersen et al., 2021), and PyMOL (PyMOL Molecular Graphics System, Version 2.0, Schrödinger, LLC).

Protein preparation

Protein preparation was conducted using the Protein Preparation Wizard (PPW) (Purushotham et al., 2022) and OPLS4 force field. Bond orders were assigned to atoms based on the CCD database, with zero bond orders given to bonded metals. Missing hydrogen atoms were inserted, and disulfide bonds were placed appropriately. During preprocessing, structural refinement was performed with Maestro's Prime utility, optimizing and adding any missing side chains and residues. Missing residues were formulated by combining SEQRS information from the PDB files and optimized using Prime's ePLOP module. The ionization state of all heterogeneous groups, including ligands, bound metals, and charged amino acids, were determined using the EpiK tool at a pH range of 7.0 ± 2.0. Subsequent force field minimization allowed for water sampling and basic restraint minimization, during which only hydrogen atoms could be freely reduced.

The hydrogen bonding (H-bond) network underwent significant modification. The terminal chi angle for Asn, Gln, and His was sampled through 180-degree flips, altering their spatial H-bonding capabilities without affecting the fit to electron density. The neutral and protonated states of His, Asp, and Glu, as well as two His tautomers, were sampled. Hydrogens on hydroxyls and thiols were also analyzed to enhance the H-bond network. Finally, the ProtAssign method was employed in two modes: a "regular" mode, which completed in seconds, and an "exhaustive" mode that considered many more states and could take minutes or hours, depending on the H-bond network complexity.

Ligand Preparation

The two-dimensional SDF structures of carbamylcholine (CCh), acetylcholine (ACh), epibatidine (Ebt) and epiboxidine (Ebx) were retrieved from the PUBCHEM database. LigPrep (LigPrep, Maestro 11.2.014, Schrödinger LLC) was utilized to construct ligands, produce stereoisomers, and generate tautomers using the OPLS46 force field. Additionally, the Epik module was employed to desalt and protonate the ligands at pH 7.0. Default values were applied to the remaining parameters, and LigPrep was also used to prepare the ligands ACh, CCh, Ebt, and Ebx, with the option "retain specified chiralities" engaged.

In terms of ligand state assessment, Epik can calculate a penalty to quantify the energy cost of forming each state in solution based on the Hammett and Taft methods. This EpiK state penalty is entirely compatible with the GlideScore used for docking, as it is computed in kcal/mol units. This compatibility facilitates the examination of how the EpiK state penalty affects the GlideScore. The DockingScore in Glide represents the total of the GlideScore and the Epik state penalty and served as the basis for final ranking and enrichment evaluation. Furthermore, Epik offers a technique for handling metal binding states, involving a change in the pH range within which the state is generated. This approach underscores the comprehensive considerations made in preparing the ligands for docking and subsequent analyses.

Grid Generation and Molecular Docking

The receptor grid complex of 6UWZ.pdb was generated after removing alpha-bungarotoxin from the binding pocket using Glide (Glide, Maestro 11.2.014, Schrödinger LLC). A virtual grid box with dimensions 20Å × 20Å × 20 Å was formed, centered within the C and F loops in the α-Δ binding site of the energy-minimized resting state. This grid box was used to generate a receptor grid, and the default values were assigned for other parameters. Docking was performed using the ligand docking wizard built into the Glide module of Schrödinger, with the default scaling factor and partial charge cutoff set to 0.80 and 0.15, respectively. The docking procedure consisted of two stages, extra precision (XP) followed by post-processing with prime MM-GBSA. The best dock poses were selected based on dock score and MM-GBSA energy for further investigation.

Molecular Dynamics Simulations

MD simulations were conducted using the Amber22 software suite within the Amber module as detailed elsewhere (Singh et al., 2021; Srivastava et al., 2022). Ligand topology was prepared via the Leap module in AmberTools22, employing force field ff19SB (Tian et al., 2020) and the Generalized Amber Force Field (GAFF) (Vassetti et al., 2019). The AM1-BCC strategy and GAFF2 were used to assign atomic charges and additional parameters. Before simulation, the systems were minimized and equilibrated following a five-step minimization process, with each step involving 10,000 energy minimization steps. Systems were heated under NVT ensembles in two consecutive runs from 0–300 K for 1 ns each, followed by a 1 ns simulation at 300 K and 1 bar pressure under the NPT ensemble for equilibration. An additional 5 ns equilibration was performed before the 200 ns production MD for each system, conducted under periodic boundary conditions (PBCs) and utilizing an NPT ensemble with 300 K and 1 bar pressure. Long-range electrostatic interactions were treated using the particle mesh Ewald method (PME), including a direct space cutoff of 12.0 Å and van der Waals interactions. In production MD, a time step of 2.0 fs was employed, and the SHAKE algorithm was used to keep bond lengths at equilibrium. Isobaric (NPT) conditions were maintained using the Berendsen barostat, with temperature monitored by a Langevin thermostat. Coordinates from the production MD were recorded in the trajectory file every 20 ps, resulting in a minimum of 10,000 frames. Trajectories were analyzed using amber-tools CPPTRAJ (Roe & Cheatham, 2013), and further analysis and figure generation were completed with VMD, Pymol, Xmgrace and ChimeraX. To ensure reproducibility, MD trajectories were generated in triplicate.

Cluster Analysis

Cluster analysis of the ligand was performed using TCL scripts within the Visual Molecular Dynamics (VMD) software, as described elsewhere (Mittal, Tonk, et al., 2021). In brief, this script automates the identification of frames from the most stable conformations based on PCA minima. Using these frames as input, the algorithm employed RMSD values of ligand positions to cluster similar orientations. Specifically, clusters with an RMSD of ≤ 1Å were considered to share a similar ligand orientation. Frames that did not fit into these top clusters were automatically excluded by the script.

Principal Component Analysis (PCA) and Free Energy Landscape (FEL)

PCA identifies collective motions in atomic-level simulations of macromolecules (Mittal, Srivastava, et al., 2021; Srivastava et al., 2022). It emphasizes significant patterns by reducing noise in MD simulations, revealing essential dynamics underlying conformational changes. All equilibrated MD simulation trajectories were analyzed by PCA computations using the CPPTRAJ algorithm in Amber tools.

Prior to PCA, least-square fitting of the protein's Cα atoms was carried out with respect to a reference structure (average protein coordinates) to eliminate rotational and translational degrees of freedom in the simulation box. A positional covariance matrix C (of dimensions $3N \times 3N$) was constructed using the Cα atom coordinates, and this matrix was diagonalized to produce eigenvectors (directions of motion) and eigenvalues (magnitudes). The elements of the covariance matrix C were obtained using:

$$C_i = \langle (X_i - \langle X_i \rangle)(X_j - \langle X_j \rangle) \rangle \quad (i, j=1,2,3.....,3N), \qquad \text{(Eq. 1)}$$

where X_i and X_j are the Cartesian coordinates of the Cα atoms, and N is the number of Cα atoms. The ⟨⟩ notation represents the ensemble average of atomic positions in Cartesian space. The resulting principal components (eigenvectors) were sorted by the total motion they captured, generating 3N eigenvectors. The free energy landscapes (FELs; FIg.3) were created using the "g_sham" module in GROMACS, based on the probability distribution of the top two principal components (PCs). The FEL plot aids in visualizing possible conformations and corresponding energy levels. The free energy values (G) were calculated as

$$G_i = -kT \ln(N_i/N_{max}) \qquad \text{(Eq. 2)}$$

where k is the Boltzmann constant, T is the absolute temperature of the simulated system (300 K), N_i is the population of bin i, and N_{max} is the population of the most-populated bin.

Binding Free Energy Calculation

The binding free energy of the protein-ligand docked complex (ΔG_{bind}) was calculated in two stages, after docking (using MM-GBSA in the Prime module of Schrödinger) (Mittal, Tonk, et al., 2021; Purushotham et al., 2022) and after MD simulation on equilibrated MD trajectories (using MM-PBSA/-GBSA in AMBER22).

After docking, for the static docked pose of the protein-ligand complex the MM-GBSA binding energy calculation was performed using the OPLS4 force field and the variable-dielectric generalized Born (VSGB) model in the Prime MM-GBSA module in Schrödinger 2022. We used ΔG_{bind_dock} to rank protein-ligand docked complexes, selecting those with the highest negative values and dock scores as the best ligands for further studies. After MD Simulation, in the MD-equilibrated system binding energies were calculated through the MM-PBSA/-GBSA protocol, implemented in AMBER22. This was performed over the most stable clustered poses extracted from the equilibrated trajectory at minima m1, m2, and m3 on the free energy landscape (FEL) over a 200 ns time frame. AMBER utilizes the conventional g_mmpbsa module for MM-PBSA calculations using MM-PBSA.py script. These methods calculate the energies of electrostatic interactions, van der Waals interactions, polar solvation, and non-polar solvation in the equilibrated trajectory using a single trajectory protocol (STP). The binding energy of each protein-ligand complex (ΔG_{bind}) was calculated as

$$G_{bind} = \Delta G_{complex} - \Delta G_{protein} - \Delta G_{ligand}$$

where $\Delta G_{complex}$, $\Delta G_{protein}$, and ΔG_{ligand} represent the absolute free energies of the complex, protein, and ligand systems, respectively. Additional terms, such as ΔH (enthalpy), T and ΔS (temperature and total solute entropy), ΔG_{gas} (total gas phase energy), and ΔG_{solv} (solvation energy), contribute to the calculation.

The Poisson-Boltzmann calculations were performed using an internal PBSA solver in Sander, while Generalized Born ESURF was calculated using 'LCPO' surface areas. The vibrational mode entropy contributions (TΔS) for protein-ligand interactions were calculated and averaged using normal-mode analysis in Amber. The entropy term provides insights into the disorder within the system, as well as how this disorder changes during the binding process. This value was added to

the enthalpy term computed by the MM-PBSA method to determine the absolute binding free energy (ΔG_{bind}). These comprehensive calculations allowed for a precise evaluation of the interactions between the protein and ligand, providing valuable insights into the binding process and its energetic characteristics.

Pocket Volume Calculation

To investigate the variations in binding site volume across all four agonist-bound cases, pocket volume analysis was carried out using POVME3.0 (Wagner et al., 2017). From each of the four systems, frames were extracted at consistent intervals with a stride of 2.0, culminating in representative sets of 5000 protein structures for every system. Before commencing the volume calculation, the trajectory was aligned, and frames were selected from VMD, serving as the initial input for this method. Subsequently, an inclusion region was defined, encapsulating all binding pocket conformations within the trajectory. This region's definition involved building a sphere upon which the inclusion grid-points were computed, using different atoms of the ligand for this calculation.

References

Auerbach A (2020) **Pathways for nicotinic receptor desensitization** *J Gen Physiol* **152** https://doi.org/10.1085/jgp.202012639

Basak S., Kumar A., Ramsey S., Gibbs E., Kapoor A., Filizola M., Chakrapani S (2020) **High-resolution structures of multiple 5-HT(3A)R-setron complexes reveal a novel mechanism of competitive inhibition** *Elife* **9** https://doi.org/10.7554/eLife.57870

Beene D. L., Brandt G. S., Zhong W., Zacharias N. M., Lester H. A., Dougherty D. A (2002) **Cation-pi interactions in ligand recognition by serotonergic (5-HT3A) and nicotinic acetylcholine receptors: the anomalous binding properties of nicotine** *Biochemistry* **41**:10262–10269 https://doi.org/10.1021/bi020266d

Bennett W. S., Steitz T. A (1978) **Glucose-induced conformational change in yeast hexokinase** *Proc Natl Acad Sci U S A* **75**:4848–4852 https://doi.org/10.1073/pnas.75.10.4848

Blum A. P., Lester H. A., Dougherty D. A (2010) **Nicotinic pharmacophore: the pyridine N of nicotine and carbonyl of acetylcholine hydrogen bond across a subunit interface to a backbone NH** *Proc Natl Acad Sci U S A* **107**:13206–13211 https://doi.org/10.1073/pnas.1007140107

Brown F. K., Kollman P. A (1987) **Molecular dynamics simulations of "loop closing" in the enzyme triose phosphate isomerase** *J Mol Biol* **198**:533–546 https://doi.org/10.1016/0022-2836(87)90298-1

Bruhova I., Auerbach A (2017) **Molecular recognition at cholinergic synapses: acetylcholine versus choline** *J Physiol* **595**:1253–1261 https://doi.org/10.1113/JP273291

Case D. A., Cheatham T. E., Darden T., Gohlke H., Luo R., Merz K. M., Onufriev A., Simmerling C., Wang B., Woods R. J. (2005) **The Amber biomolecular simulation programs** *J Comput Chem* **26**:1668–1688 https://doi.org/10.1002/jcc.20290

Celie P. H., van Rossum-Fikkert S. E., van Dijk W. J., Brejc K., Smit A. B., Sixma T. K. (2004) **Nicotine and carbamylcholine binding to nicotinic acetylcholine receptors as studied in AChBP crystal structures** *Neuron* **41**:907–914 https://doi.org/10.1016/s0896-6273(04)00115-1

Chang Y., Weiss D. S (2002) **Site-specific fluorescence reveals distinct structural changes with GABA receptor activation and antagonism** *Nat Neurosci* **5**:1163–1168 https://doi.org/10.1038/nn926

Chen S., Zhao Y., Wang Y., Shekhar M., Tajkhorshid E., Gouaux E (2017) **Activation and Desensitization Mechanism of AMPA Receptor-TARP Complex by Cryo-EM** *Cell* **170**:1234–1246 https://doi.org/10.1016/j.cell.2017.07.045

Cheng X., Wang H., Grant B., Sine S. M., McCammon J. A (2006) **Targeted molecular dynamics study of C-loop closure and channel gating in nicotinic receptors** *PLoS Comput Biol* **2** https://doi.org/10.1371/journal.pcbi.0020134

Du J., Lu W., Wu S., Cheng Y., Gouaux E (2015) **Glycine receptor mechanism elucidated by electron cryo-microscopy** *Nature* **526**:224–229 https://doi.org/10.1038/nature14853

Furukawa H., Singh S. K., Mancusso R., Gouaux E (2005) **Subunit arrangement and function in NMDA receptors** *Nature* **438**:185–192 https://doi.org/10.1038/nature04089

Gay E. A., Yakel J. L (2007) **Gating of nicotinic ACh receptors; new insights into structural transitions triggered by agonist binding that induce channel opening** *J Physiol* **584**:727–733 https://doi.org/10.1113/jphysiol.2007.142554

Genheden S., Ryde U (2015) **The MM/PBSA and MM/GBSA methods to estimate ligand-binding affinities** *Expert Opin Drug Discov* **10**:449–461 https://doi.org/10.1517/17460441.2015.1032936

Gharpure A., Teng J., Zhuang Y., Noviello C. M., Walsh R. M., Cabuco R., Howard R. J., Zaveri N. T., Lindahl E., Hibbs R. E (2019) **Agonist Selectivity and Ion Permeation in the alpha3beta4 Ganglionic Nicotinic Receptor** *Neuron* **104**:501–511 https://doi.org/10.1016/j.neuron.2019.07.030

Grosman C., Auerbach A (2001) **The dissociation of acetylcholine from open nicotinic receptor channels** *Proc Natl Acad Sci U S A* **98**:14102–14107 https://doi.org/10.1073/pnas.251402498

Grosman C., Zhou M., Auerbach A (2000) **Mapping the conformational wave of acetylcholine receptor channel gating** *Nature* **403**:773–776 https://doi.org/10.1038/35001586

Gupta S., Chakraborty S., Vij R., Auerbach A (2017) **A mechanism for acetylcholine receptor gating based on structure, coupling, phi, and flip** *J Gen Physiol* **149**:85–103 https://doi.org/10.1085/jgp.201611673

Hansen S. B., Sulzenbacher G., Huxford T., Marchot P., Taylor P., Bourne Y (2005) **Structures of Aplysia AChBP complexes with nicotinic agonists and antagonists reveal distinctive binding interfaces and conformations** *Embo Journal* **24**:3635–3646 https://doi.org/10.1038/sj.emboj.7600828

Hibbs R. E., Gouaux E (2011) **Principles of activation and permeation in an anion-selective Cys-loop receptor** *Nature* **474**:54–60 https://doi.org/10.1038/nature10139

Hibbs R. E., Sulzenbacher G., Shi J., Talley T. T., Conrod S., Kem W. R., Taylor P., Marchot P., Bourne Y (2009) **Structural determinants for interaction of partial agonists with acetylcholine binding protein and neuronal alpha7 nicotinic acetylcholine receptor** *Embo Journal* **28**:3040–3051 https://doi.org/10.1038/emboj.2009.227

Hou T., Wang J., Li Y., Wang W (2011) **Assessing the performance of the MM/PBSA and MM/GBSA methods. 1. The accuracy of binding free energy calculations based on molecular dynamics simulations** *Journal of Chemical Information and Modeling* **51**:69–82 https://doi.org/10.1021/ci100275a

Huang W. *et al.* (2015) **Structural insights into micro-opioid receptor activation** *Nature* **524**:315–321 https://doi.org/10.1038/nature14886

Humphrey W., Dalke A., Schulten K (1996) **VMD: visual molecular dynamics** *J Mol Graph* **14**:33–38 https://doi.org/10.1016/0263-7855(96)00018-5

Indurthi D., Auerbach A (2021) **Agonist Efficiency Estimated from Concentration Response Curve** *Biophysical Journal* **120**:57–57

Indurthi D. C., Auerbach A (2023) **Agonist efficiency links binding and gating in a nicotinic receptor** *Elife* **12** https://doi.org/10.7554/eLife.86496

Jackson M. B (1986) **Kinetics of unliganded acetylcholine receptor channel gating** *Biophys J* **49**:663–672 https://doi.org/10.1016/S0006-3495(86)83693-1

Jadey S., Auerbach A (2012) **An integrated catch-and-hold mechanism activates nicotinic acetylcholine receptors** *J Gen Physiol* **140**:17–28 https://doi.org/10.1085/jgp.201210801

Klabunde T., Petrassi H. M., Oza V. B., Raman P., Kelly J. W., Sacchettini J. C (2000) **Rational design of potent human transthyretin amyloid disease inhibitors** *Nat Struct Biol* **7**:312–321 https://doi.org/10.1038/74082

Klei H. E. *et al.* (2007) **X-ray crystal structures of human immunodeficiency virus type 1 protease mutants complexed with atazanavir** *J Virol* **81**:9525–9535 https://doi.org/10.1128/JVI.02503-05

Kollman P. A. *et al.* (2000) **Calculating structures and free energies of complex molecules: combining molecular mechanics and continuum models** *Acc Chem Res* **33**:889–897 https://doi.org/10.1021/ar000033j

Ma W., Tang C., Lai L (2005) **Specificity of trypsin and chymotrypsin: loop-motion-controlled dynamic correlation as a determinant** *Biophys J* **89**:1183–1193 https://doi.org/10.1529/biophysj.104.057158

Mittal L., Srivastava M., Kumari A., Tonk R. K., Awasthi A., Asthana S (2021) **Interplay among Structural Stability, Plasticity, and Energetics Determined by Conformational Attuning of Flexible Loops in PD-1** *Journal of Chemical Information and Modeling* **61**:358–384 https://doi.org/10.1021/acs.jcim.0c01080

Mittal L., Tonk R. K., Awasthi A., Asthana S (2021) **Targeting cryptic-orthosteric site of PD-L1 for inhibitor identification using structure-guided approach** *Arch Biochem Biophys* **713** https://doi.org/10.1016/j.abb.2021.109059

Mukhtasimova N., Free C., Sine S. M (2005) **Initial coupling of binding to gating mediated by conserved residues in the muscle nicotinic receptor** *J Gen Physiol* **126**:23–39 https://doi.org/10.1085/jgp.200509283

Munro L., Ladefoged L. K., Padmanathan V., Andersen S., Schiott B., Kristensen A. S (2019) **Conformational Changes in the 5-HT(3A) Receptor Extracellular Domain Measured by Voltage-Clamp Fluorometry** *Molecular Pharmacology* **96**:720–734 https://doi.org/10.1124/mol.119.116657

Muroi Y., Theusch C. M., Czajkowski C., Jackson M. B (2009) **Distinct structural changes in the GABAA receptor elicited by pentobarbital and GABA** *Biophys J* **96**:499–509 https://doi.org/10.1016/j.bpj.2008.09.037

Nayak T. K., Auerbach A (2017) **Cyclic activation of endplate acetylcholine receptors** *Proc Natl Acad Sci U S A* **114**:11914–11919 https://doi.org/10.1073/pnas.1711228114

Nayak T. K., Chakraborty S., Zheng W. J., Auerbach A (2016) **Structural correlates of affinity in fetal versus adult endplate nicotinic receptors** *Nature Communications* **7** https://doi.org/10.1038/ncomms11352

Nayak T. K., Purohit P. G., Auerbach A (2012) **The intrinsic energy of the gating isomerization of a neuromuscular acetylcholine receptor channel** *J Gen Physiol* **139**:349–358 https://doi.org/10.1085/jgp.201110752

Nayak T. K., Vij R., Bruhova I., Shandilya J., Auerbach A (2019) **Efficiency measures the conversion of agonist binding energy into receptor conformational change** *J Gen Physiol* **151**:465–477 https://doi.org/10.1085/jgp.201812215

Nickbarg E. B., Davenport R. C., Petsko G. A., Knowles J. R (1988) **Triosephosphate isomerase: removal of a putatively electrophilic histidine residue results in a subtle change in catalytic mechanism** *Biochemistry* **27**:5948–5960 https://doi.org/10.1021/bi00416a019

Noviello C. M., Gharpure A., Mukhtasimova N., Cabuco R., Baxter L., Borek D., Sine S. M., Hibbs R. E (2021) **Structure and gating mechanism of the alpha7 nicotinic acetylcholine receptor** *Cell* **184**:2121–2134 https://doi.org/10.1016/j.cell.2021.02.049

Oostenbrink C., Villa A., Mark A. E., van Gunsteren W. F. (2004) **A biomolecular force field based on the free enthalpy of hydration and solvation: the GROMOS force-field parameter sets 53A5 and 53A6** *J Comput Chem* **25**:1656–1676 https://doi.org/10.1002/jcc.20090

Padgett C. L., Hanek A. P., Lester H. A., Dougherty D. A., Lummis S. C (2007) **Unnatural amino acid mutagenesis of the GABA(A) receptor binding site residues reveals a novel cation-pi interaction between GABA and beta 2Tyr97** *Journal of Neuroscience* **27**:886–892 https://doi.org/10.1523/JNEUROSCI.4791-06.2007

Pettersen E. F., Goddard T. D., Huang C. C., Meng E. C., Couch G. S., Croll T. I., Morris J. H., Ferrin T. E (2021) **UCSF ChimeraX: Structure visualization for researchers, educators, and developers** *Protein Sci* **30**:70–82 https://doi.org/10.1002/pro.3943

Plapp B. V (2010) **Conformational changes and catalysis by alcohol dehydrogenase** *Arch Biochem Biophys* **493**:3–12 https://doi.org/10.1016/j.abb.2009.07.001

Pless S. A., Hanek A. P., Price K. L., Lynch J. W., Lester H. A., Dougherty D. A., Lummis S. C (2011) **A cation-pi interaction at a phenylalanine residue in the glycine receptor binding site is conserved for different agonists** *Molecular Pharmacology* **79**:742–748

Pless S. A., Lynch J. W (2009) **Ligand-specific conformational changes in the alpha1 glycine receptor ligand-binding domain** *J Biol Chem* **284**:15847–15856 https://doi.org/10.1074/jbc.M809343200

Polovinkin L. *et al.* (2018) **Conformational transitions of the serotonin 5-HT(3) receptor** *Nature* **563**:275–279 https://doi.org/10.1038/s41586-018-0672-3

Purohit P., Auerbach A (2009) **Unliganded gating of acetylcholine receptor channels** *Proc Natl Acad Sci U S A* **106**:115–120 https://doi.org/10.1073/pnas.0809272106

Purohit P., Auerbach A (2013) **Loop C and the mechanism of acetylcholine receptor-channel gating** *J Gen Physiol* **141**:467–478 https://doi.org/10.1085/jgp.201210946

Purohit P., Bruhova I., Gupta S., Auerbach A (2014) **Catch-and-Hold Activation of Muscle Acetylcholine Receptors Having Transmitter Binding Site Mutations** *Biophysical Journal* **107**:88–99 https://doi.org/10.1016/j.bpj.2014.04.057

Purohit P., Gupta S., Jadey S., Auerbach A (2013) **Functional anatomy of an allosteric protein** *Nature Communications* **4** https://doi.org/10.1038/ncomms3984

Purushotham N., Singh M., Paramesha B., Kumar V., Wakode S., Banerjee S. K., Poojary B., Asthana S (2022) **Design and synthesis of amino acid derivatives of substituted benzimidazoles and pyrazoles as Sirt1 inhibitors** *RSC Adv* **12**:3809–3827 https://doi.org/10.1039/d1ra06149f

Rahman M. M., Basta T., Teng J., Lee M., Worrell B. T., Stowell M. H. B., Hibbs R. E (2022) **Structural mechanism of muscle nicotinic receptor desensitization and block by curare** *Nat Struct Mol Biol* **29**:386–394 https://doi.org/10.1038/s41594-022-00737-3

Rahman M. M., Teng J., Worrell B. T., Noviello C. M., Lee M., Karlin A., Stowell M. H. B., Hibbs R. E (2020) **Structure of the Native Muscle-type Nicotinic Receptor and Inhibition by Snake Venom Toxins** *Neuron* **106**:952–962 https://doi.org/10.1016/j.neuron.2020.03.012

Rasmussen S. G. *et al.* (2011) **Crystal structure of the beta2 adrenergic receptor-Gs protein complex** *Nature* **477**:549–555 https://doi.org/10.1038/nature10361

Rastelli G., Del Rio A., Degliesposti G., Sgobba M (2010) **Fast and accurate predictions of binding free energies using MM-PBSA and MM-GBSA** *J Comput Chem* **31**:797–810 https://doi.org/10.1002/jcc.21372

Roe D. R., Cheatham T. E. (2013) **PTRAJ and CPPTRAJ: Software for Processing and Analysis of Molecular Dynamics Trajectory Data** *J Chem Theory Comput* **9**:3084–3095 https://doi.org/10.1021/ct400341p

Shang Y., Yeatman H. R., Provasi D., Alt A., Christopoulos A., Canals M., Filizola M (2016) **Proposed Mode of Binding and Action of Positive Allosteric Modulators at Opioid Receptors** *ACS Chem Biol* **11**:1220–1229 https://doi.org/10.1021/acschembio.5b00712

Sigel E., Steinmann M. E (2012) **Structure, function, and modulation of GABA(A) receptors** *J Biol Chem* **287**:40224–40231 https://doi.org/10.1074/jbc.R112.386664

Singh M., Srivastava M., Wakode S. R., Asthana S (2021) **Elucidation of Structural Determinants Delineates the Residues Playing Key Roles in Differential Dynamics and Selective Inhibition of Sirt1-3** *Journal of Chemical Information and Modeling* **61**:1105–1124 https://doi.org/10.1021/acs.jcim.0c01193

Srivastava M., Mittal L., Kumari A., Agrahari A. K., Singh M., Mathur R., Asthana S (2022) **Characterizing (un)binding mechanism of USP7 inhibitors to unravel the cause of enhanced binding potencies at allosteric checkpoint** *Protein Sci* **31** https://doi.org/10.1002/pro.4398

Sun H., Li Y., Tian S., Xu L., Hou T (2014) **Assessing the performance of MM/PBSA and MM/GBSA methods. 4. Accuracies of MM/PBSA and MM/GBSA methodologies evaluated by various simulation protocols using PDBbind data set** *Phys Chem Chem Phys* **16**:16719–16729 https://doi.org/10.1039/c4cp01388c

Tarvin R. D., Borghese C. M., Sachs W., Santos J. C., Lu Y., O'Connell L. A., Cannatella D. C., Harris R. A., Zakon H. H (2017) **Interacting amino acid replacements allow poison frogs to evolve epibatidine resistance** *Science* **357**:1261–1266 https://doi.org/10.1126/science.aan5061

Tian C. *et al.* (2020) **ff19SB: Amino-Acid-Specific Protein Backbone Parameters Trained against Quantum Mechanics Energy Surfaces in Solution** *J Chem Theory Comput* **16**:528–552 https://doi.org/10.1021/acs.jctc.9b00591

Tripathy S., Zheng W., Auerbach A (2019) **A single molecular distance predicts agonist binding energy in nicotinic receptors** *J Gen Physiol* **151**:452–464 https://doi.org/10.1085/jgp.201812212

Unwin N (1993) **Nicotinic acetylcholine receptor at 9 A resolution** *J Mol Biol* **229**:1101–1124 https://doi.org/10.1006/jmbi.1993.1107

Vassetti D., Pagliai M., Procacci P (2019) **Assessment of GAFF2 and OPLS-AA General Force Fields in Combination with the Water Models TIP3P, SPCE, and OPC3 for the Solvation Free Energy of Druglike Organic Molecules** *J Chem Theory Comput* **15**:1983–1995 https://doi.org/10.1021/acs.jctc.8b01039

Wagner J. R., Sorensen J., Hensley N., Wong C., Zhu C., Perison T., Amaro R. E (2017) **POVME 3.0: Software for Mapping Binding Pocket Flexibility** *J Chem Theory Comput* **13**:4584–4592 https://doi.org/10.1021/acs.jctc.7b00500

Walsh R. M., Roh S. H., Gharpure A., Morales-Perez C. L., Teng J., Hibbs R. E (2018) **Structural principles of distinct assemblies of the human alpha4beta2 nicotinic receptor** *Nature* **557**:261–265 https://doi.org/10.1038/s41586-018-0081-7

Wlodawer A., Erickson J. W (1993) **Structure-based inhibitors of HIV-1 protease** *Annu Rev Biochem* **62**:543–585 https://doi.org/10.1146/annurev.bi.62.070193.002551

Xiu X., Puskar N. L., Shanata J. A., Lester H. A., Dougherty D. A (2009) **Nicotine binding to brain receptors requires a strong cation-pi interaction** *Nature* **458**:534–537 https://doi.org/10.1038/nature07768

Zarkadas E., Pebay-Peyroula E., Thompson M. J., Schoehn G., Uchanski T., Steyaert J., Chipot C., Dehez F., Baenziger J. E., Nury H (2022) **Conformational transitions and ligand-binding to a muscle-type nicotinic acetylcholine receptor** *Neuron* **110**:1358–1370 https://doi.org/10.1016/j.neuron.2022.01.013

Zhong W., Gallivan J. P., Zhang Y., Li L., Lester H. A., Dougherty D. A (1998) **From ab initio quantum mechanics to molecular neurobiology: a cation-pi binding site in the nicotinic receptor** *Proc Natl Acad Sci U S A* **95**:12088–12093 https://doi.org/10.1073/pnas.95.21.12088

Article and author information

Mrityunjay Singh
Computational Biophysics and CADD Group, Computational and Mathematical Biology Center, Translational Health Science and Technology Institute, NCR Biotech Science Cluster, Faridabad 121001, India

Dinesh C. Indurthi
Department of Physiology and Biophysics, University at Buffalo, State University of New York, Buffalo, United States
For correspondence: dinesh.indurthi@gmail.com

Lovika Mittal
Computational Biophysics and CADD Group, Computational and Mathematical Biology Center, Translational Health Science and Technology Institute, NCR Biotech Science Cluster, Faridabad 121001, India

Anthony Auerbach
Department of Physiology and Biophysics, University at Buffalo, State University of New York, Buffalo, United States
For correspondence: anthony.auerbach@gmail.com

Shailendra Asthana
Computational Biophysics and CADD Group, Computational and Mathematical Biology Center, Translational Health Science and Technology Institute, NCR Biotech Science Cluster, Faridabad 121001, India
For correspondence: sasthana@thsti.res.in

Copyright

Editors

Reviewing Editor
Marcel Goldschen-Ohm
University of Texas at Austin, Austin, United States of America

Senior Editor
Kenton Swartz
National Institute of Neurological Disorders and Stroke, National Institutes of Health, Bethesda, United States of America

Reviewer #1 (Public Review):

Summary:
This useful work provides insight into agonist binding to muscle nicotinic receptors. The authors want to understand the fundamental steps in ligand binding to muscle nicotinic receptors using computational methods. The study builds on a large basis of empirical studies of the various states involved in receptor activation. However, the evidence supporting the conclusions is incomplete, because little support is available for the starting structures that are derived from ligand docking. This work is a useful starting point for more detailed work on ligand binding to this important class of receptors.

Strengths:
The strengths include the number of ligands tried, and the relation to the mature analysis of the receptor function.

Weaknesses:
The weaknesses are the brevity of the simulations, the concomitant lack of scope of the

simulations, the lack of depth in the analysis, and the incomplete relation to other relevant work.

- https://doi.org/10.7554/eLife.92418.1.sa3

Reviewer #2 (Public Review):

Summary:
The aim of this manuscript is to use molecular dynamics (MD) simulations to describe the conformational changes of the neurotransmitter binding site of a nicotinic receptor. The study uses a simplified model including the alpha-delta subunit interface of the extracellular domain of the channel and describes the binding of four agonists to observe conformational changes during the weak-to-strong affinity transition.

Strength:
The 200 ns-long simulations of this model suggest that the agonist rotates about its centre in a 'flip' motion, while loop C 'flops' to restructure the site. The changes appear to be reproduced across simulations and different ligands and are thus a strong point of the study.

Weaknesses:
After carrying out all-atom molecular dynamics, the authors revert to a model of binding using continuum Poisson-Boltzmann, surface area, and vibrational entropy. The motivations for and limitations associated with this approximate model for the thermodynamics of binding, rather than using modern atomistic MD free energy methods (that would fully incorporate configurational sampling of the protein, ligand, and solvent) could be provided. Despite this, the authors report a correlation between their free energy estimates and those inferred from the experiment. This did, however, reveal shortcomings for two of the agonists. The authors mention their trouble getting correlation to experiment for Ebt and Ebx and refer to up to 130% errors in free energy. But this is far worse than a simple proportional error, because -24 Vs -10 kcal/mol is a massive overestimation of free energy, as would be evident if the authors were to instead express results in terms of KD values (which would have an error exceeding a billion fold). The MD analysis could be improved with better measures of convergence, as well as a more careful discussion of free energy maps as a function of identified principal components, as described below. Overall, however, the study has provided useful observations and interpretations of agonist binding that will help understand pentameric ligand-gated ion channel activation.

Main points:
Regarding the choice of model, some further justification of the reduced 2 subunit ECD-only model could be given. On page 5 the authors argue that, because binding free energies are independent of energy changes outside the binding pocket, they could remove the TMD and study only an ECD subunit dimer. While the assumption of distant interactions being small seems somewhat reasonable, provided conformational changes are limited and localised, how do we know the packing of TMD onto the ECD does not alter the ability of the alpha-delta interface to rearrange during weak or strong binding? They further write that "fluctuations observed at the base of the ECD were anticipated because the TMD that offers stability here was absent.". As the TMD-ECD interface is the "gating interface" that is reshaped by agonist binding, surely the TMD-ECD interface structure must affect binding. It seems a little dangerous to completely separate the agonist binding and gating infrastructure, based on some assumption of independence. Given the model was only the alpha and delta subunits and not the pentamer with TMD, I am surprised such a model was stable without some heavy restraints. The authors state that "as a further control we carried out MD simulation of a pentamer docked with ACh and found similar structural changes at the binding pocket compared to the dimer." Is this sufficient proof of the accuracy of the simplified model? How similar was the model itself with and without agonist in terms of overall RMSD and RMSD for

the subunit interface and the agonist binding site, as well as the free energy of binding to each model to compare?

Although the authors repeatedly state that they have good convergence with their MD, I believe the analysis could be improved to convince us. On page 8 the authors write that the RMSD of the system converged in under 200 ns of MD. However, I note that the graph is of the entire ECD dimer, not a measure for the local binding site region. An additional RMSD of local binding site would be much more telling. You could have a structural isomerisation in the site and not even notice it in the existing graph. On page 9 the authors write that the RMSF in Figure S2 showed instability mainly in loops C and F around the pocket. Given this flexibility at the alpha-delta interface, this is why collecting those regions into one group for the calculation of RMSD convergence analysis would have been useful. They then state "the final MD configuration (with CCh) was well-aligned with the CCh-bound cryo-EM desensitized structure (7QL6)... further demonstrating that the simulation had converged." That may suggest a change occurred that is in common with the global minimum seen in cryo EM, which is good, but does not prove the MD has "converged". I would also rename Figure S3 accordingly.

The authors draw conclusions about the dominant states and pathways from their PCA component free energy projections that need clarification. It is important first to show data to demonstrate that the two PCA components chosen were dominant and accounted for most of the variance. Then when mapping free energy as a function of those two PCA components, to prove that those maps have sufficient convergence to be able to interpret them. Moreover, if the free energies themselves cannot be used to measure state stability (as seems to be the case), that the limitations are carefully explained. First, was PCA done on all MD trajectories combined to find a common PC1 & PC2, or were they done separately on each simulation? If so, how similar are they? The authors write "the first two principal components (PC-1 and PC-2) that capture the most pronounced C. displacements". How much of the total variance did these two components capture? The authors write the changes mostly concern loop C and loop F, but which data proves this? e.g. A plot of PC1 and PC2 over residue number might help.

The authors map the -kTln rho as a free energy for each simulation as a function of PC1 & PC2. It is important to reveal how well that PC1-2 space was sampled, and how those maps converged over time. The shapes of the maps and the relative depths of the wells look very different for each agonist. If the maps were sampled well and converged, the free energies themselves would tell us the stabilities of each state. Instead, the authors do not even mention this and instead talk about "variance" being the indicator of stability, stating that m3 is most stable in all cases. While I can believe 200ns could not converge a PC1-2 map and that meaningful delta G values might not be obtained from them, the issue of lack of sampling must be dealt with. On page 12 they write "Although the bottom of the well for 3 energy minima from PCA represent the most stable overall conformation of the protein, they do not convey direct information regarding agonist stability or orientation". The reasons why not must be explained; as they should do just that if the two order parameters PC1 and PC2 captured the slowest degrees of freedom for binding and sampling was sufficient. The authors write that "For all agonists and trajectories, m3 had the least variance (was most stable), again supporting convergence by 200 ns." Again the issue of actual free energy values in the maps needs to be dealt with. The probabilities expressed as -kTln rho in kcal/mol might suggest that m2 is the most stable. Instead, the authors base stability only on variance (I guess breadth of the well?), where m3 may be more localised in the chosen PC space, despite apparently having less preference during the MD (not the lowest free energy in the maps).

The motivations and justifications for the use of approximate PBSA energetics instead of atomistic MD free energies should be dealt with in the manuscript, with limitations more clearly discussed. Rather than using modern all-atom MD free energy methods for relative or

absolute binding free energies, the author selects clusters from their identified states and does Poisson-Boltzmann estimates (electrostatic, vdW, surface area, vibrational entropy). I do believe the following sentence does not begin to deal with the limitations of that method: "there are limitations with regard to MM-PBSA accurately predicting absolute binding free energies (Genheden & Ryde, 2015; Hou et al., 2011) that depends on the parameterization of the ligand (Oostenbrink et al., 2004)." What are the assumptions and limitations in taking continuum electrostatics (presumably with parameters for dielectric constants and their assignments to regions after discarding solvent), surface area (with its assumptions and limitations), and of course assuming vibration of a normal mode can capture entropy. On page 30, regarding their vibrational entropy estimate, they write that the "entropy term provides insights into the disorder within the system, as well as how this disorder changes during the binding process". It is important that the extent of disorder captured by the vibrational estimate be discussed, as it is not obvious that it has captured entropy involving multiple minima on the system's true 3N-dimensional energy surface, and especially the contribution from solvent disorder in bound Vs dissociated states.

As discussed above, errors in the free energy estimates need to be more faithfully represented, as fractional errors are not meaningful. On page 21 the authors write "The match improved when free energy ratios rather than absolute values were compared." But a ratio of free energies is not a typical or expected measure of error in delta G. They also write "For ACh and CCh, there is good agreement between.Gm1 and GLA and between.Gm3 and GHA. For these agonists, in silico values overestimated experimental ones only by ~8% and ~25%. The agreement was not as good for the other 2 agonists, as calculated values overestimated experimental ones by ~45%(Ebt) and ~130% (Ebt). However, the fractional overestimation was approximately the same for GLA and GHA." See the above comment on how this may misrepresent the error. On page 21 they write, in relation to their large fractional errors, that they "do not know the origin of this factor but speculate that it could be caused by errors in ligand parameterization". However the estimates from the PBSA approach are, by design, only approximate. Both errors in parameterisation (and their likely origin) and the approximate model used, need discussion.

- https://doi.org/10.7554/eLife.92418.1.sa2

Reviewer #3 (Public Review):

Summary:
The authors use docking and molecular dynamics (MD) simulations to investigate transient conformations that are otherwise difficult to resolve experimentally. The docking and simulations suggest an interesting series of events whereby agonists initially bind to the low-affinity site and then flip 180 degrees as the site contracts to its high-affinity conformation. This work will be of interest to the ion channel community and to biophysical studies of pentameric ligand-gated channels.

Strengths:
I find the premise for the simulations to be good, starting with an antagonist-bound structure as an estimate of the low affinity binding site conformation, then docking agonists into the site and using MD to allow the site to relax to a higher affinity conformation that is similar to structures in complex with agonists. I cannot speak to the details of the simulation methods, but the predictions are interesting and provide a view into what a transient conformation that is difficult to observe experimentally might be like.

Weaknesses:
Although the match in simulated vs experimental energies for two ligands was very good, the calculated energies for two other ligands were significantly different than the experiment. It

is unclear to what extent the choice of method for the energy calculations influenced the results.

A control simulation, such as for an apo site, is lacking.

- https://doi.org/10.7554/eLife.92418.1.sa1

Reviewer #4 (Public Review):

Summary:
In their manuscript "Conformational dynamics of a nicotinic receptor neurotransmitter binding site," Singh and colleagues present cogent molecular docking and dynamics simulations to explore the initial conformational changes associated with agonist binding in the muscle nicotinic acetylcholine receptor, aligned with the extensive experimental literature on this system. Their central findings are of a consistently preferred pose for agonists upon initial association with a resting channel, followed by a dramatic rotation of the ligand and contraction of a critical loop over the binding site. Principal component analysis also suggests the formation of an intermediate complex, not yet captured in structural studies. Binding free energy calculations are consistent with the evolution of a higher-affinity complex following agonist binding, with a ligand efficiency notably similar to experimental values. Snapshot comparisons provide a structural rationale for these changes on the basis of pocket volume, hydration, and rearrangement of key residues at the subunit interface.

Strengths:
Docking results are clearly presented and remarkably consistent. Simulations are produced in triplicate with each of four different agonists, providing an informative basis for internal validation. They identify an intriguing transition in ligand pose, not well documented in experimental structures, and potentially applicable to mechanistic or even pharmacological modeling of this and related receptor systems. The paper seems a notable example of integrating quantitative structure-function analysis with systematic computational modeling and simulations, likely applicable to the wider journal audience.

Weaknesses:
Timescales (200 ns) do not capture global rearrangements of the extracellular domain, let alone gating transitions of the channel pore, though this work may provide a launching point for more extended simulations. A more general concern is the reproducibility of the simulations, and how representative states are defined. It is not clear whether replicates were included in principal component analysis or subsequent binding energy calculations, nor how simulation intervals were associated with specific states. Structural analysis largely focuses on snapshots, with limited direct evidence of consistency across replicates or clusters. Figure legends and tables could be clarified.

- https://doi.org/10.7554/eLife.92418.1.sa0